Communications

Structural and Compositional Control in {M$_{12}$} Cobalt and Nickel Coordination Clusters Detected Magnetochemically and with Cryospray Mass Spectrometry**

Geoffrey J. T. Cooper, Graham N. Newton, Paul Kögerler, De-Liang Long, Larry Engelhardt, Marshall Luban, and Leroy Cronin**

Full compositional and structural control in the high-nuclearity coordination clusters of transition-metal cations is a crucial synthetic target, and is motivated by these species' complex electronic and magnetic properties which single them out as metalloenzyme models,[1] nanoscale containers and catalysts,[2] quantum computing components,[3] and molecular magnets.[4] Strategies for their synthesis range from the use of multifunctional organic ligands[5] to the controlled production of molecular sections of solid-state structures, such as those of transition-metal oxides.[6] In most instances the resulting metal frameworks are derived from various archetypal condensed substructures, such as (distorted) M$_4$L$_4$ cubanes (M = metal, L = O, N, etc.). Such cubanes constitute a class of discrete compounds such as complexes based on Ni$_4$O$_4$ or Co$_4$O$_4$ structures, which themselves represent sections of their respective oxides. For the past four decades, these species have been studied as precursors for metal oxide nanoparticles,[7] novel magnetic materials,[8] and polymerization catalysts.[9] Coordination complexes of higher nuclearity, such as {Ni$_{11}$},[10] or {Co$_{14}$}[11] frequently comprise corner-, edge-, or face-sharing aggregates of M$^{II}_4$O$^{II}_4$. As such, the generation of isostructural metal–ligand frameworks is especially important as they allow systematic, comparative studies of their complex magnetic phenomena and the possibility to precisely position heterometal atoms within a given architecture. However, while several almost isostructural compounds of Ni^{II} and Co^{II} exist, including M$_4$O$_4$ cubane structures, because of their very similar coordination chemistry,[12] these are invariably of low nuclearity, and systems exceeding ten metal centers are

rare.[13] Correspondingly, mixed-metal isostructures (i.e. structures incorporating both Ni^{II} and Co^{II} centers in varying ratios that are distributed over the metal framework of a coordination cluster) can be generated, yet site-specific occupation is frequently subject to binomial statistics and cannot be resolved by diffraction techniques. In such situations, as we demonstrate herein, magnetic properties can be used to discern between the possible intramolecular distribution scenarios and indicate how narrow the distribution curves are for (cocrystallizing) compositions (of the type {M$_{x-\Delta}$M′$_{y+\Delta}$}, {M$_x$M′$_y$}, {M$_{x+\Delta}$M′$_{y-\Delta}$}).

Herein, we demonstrate the use of templating and multifunctional ligands to facilitate the directed assembly of archetypal isostructural Ni$^{II}_4$O$_4$ and Co$^{II}_4$O$_4$ cubane building blocks to form high-nuclearity {Ni$_{12}$} and {Co$_{12}$} clusters.[14] These clusters comprise three M$_4$O$_4$ cubane units symmetrically arranged around a central templating carbonate anion and the intact clusters {M$_{12}$} can be detected in solution using cryospray mass spectrometry.[15] Moreover, isostructural mixed Ni:Co clusters of specific composition can be accessed since the pH value of the reaction solution (i.e. an additional reaction parameter besides the stoichiometric reaction ratio of Ni and Co) is used to differentiate the relative population of the metal sites in the {M$_{12}$} system. This approach allows us to access intermediates with discrete (i.e. non-mixed: that is $\Delta \rightarrow 0$) compositions {Ni$_{12-n}$Co$_n$} ($n = 1$, 2, …, 11)[16] which make up a series for which the resulting magnetic properties can be fine-tuned. In turn, the resulting magnetic properties allow us to identify Ni:Co-specific binding sites in the given {M$_{12}$} structure; this fact is crucial if spatial, site-specific resolution is to be utilized in the design of new functional architectures.

Central to the synthesis of the {M$_{12}$} coordination clusters is the aliphatic triamine ligand *cis,trans*-1,3,5-triaminocyclohexane (*trans*-tach) which is employed in conjunction with bridging acetate and templating carbonate ligands. *trans*-Tach[17] is particularly versatile owing to the rigidity of its cyclohexane backbone which prevents the interaction of all three amino donor groups with one single metal center and a bis(axial)–mono(equatorial) of the amine groups is invariably observed upon coordination to open-shell transition-metal cations. In our case, the *trans*-tach ligand can simultaneously act as a bis-chelating ligand while the protonated terminal *trans* amine group can also help anchor the complex into supramolecular hydrogen-bonded networks.

The {Co$_{12}$} cluster is prepared by addition of cobalt(II) acetate to a methanol solution of *trans*-tach in a 1:1 molar

[*] Dr. P. Kögerler, L. Engelhardt, Prof. M. Luban
Ames Laboratory & Department of Physics & Astronomy
Iowa State University
Ames, IA 50011 (USA)
Fax: (+1) 515-294-0689
E-mail: Kogerler@ameslab.gov

Dr. G. J. T. Cooper, G. N. Newton, Dr. D.-L. Long, Prof. L. Cronin
Department of Chemistry
The University of Glasgow
Glasgow, G12 8QQ (UK)
Fax: (+44) 141-330-4888
E-mail: L.Cronin@chem.gla.ac.uk

© 2007 Wiley-VCH Verlag GmbH & Co. KGaA, Weinheim

Angew. Chem. Int. Ed. **2007**, *46*, 1340–1344

ratio with sufficient addition of dilute perchloric (or acetic) acid to achieve pH 8.5, resulting in a purple solution from which crystals of $[Co^{II}_{12}(\textit{trans}\text{-tachH})_6(OH)_{12}(OAc)_9(CO_3)](ClO_4)_7 \cdot 12\,MeOH$ (**1**) are isolated. The analogous reaction of nickel(II) acetate with *trans*-tach in methanol at an unadjusted pH of 10.5 yields a green solution from which crystals of $[Ni^{II}_{12}(\textit{trans}\text{-tachH})_6(OMe)_{12}(OAc)_9(CO_3)](OAc)_7 \cdot 10\,MeOH \cdot 6\,H_2O$ (**2**) can be grown. Furthermore, the cluster cores of $\{Co_{12}\} = [Co_{12}(\textit{trans}\text{-tachH})_6(OH)_{12}(OAc)_9(CO_3)]^{7+}$ (**1a**) and $\{Ni_{12}\} = [Ni_{12}(\textit{trans}\text{-tachH})_6(OMe)_{12}(OAc)_9(CO_3)]^{7+}$ (**2a**) differ only in the relative amounts of μ_3-hydroxo and μ_3-methoxo groups found in the cubane units but show striking differences in the long-range ordering of

Figure 1. Structure of the {Ni$_{12}$} complex **2a** along the C_3 axis (left) and one of the three C_2 axes (right). Ni green, C gray, N blue, O red.

clusters in the crystalline state; this is partly caused by the interactions between the protonated *trans*-amino groups in *trans*-tach between adjacent clusters in the crystal lattice. The cluster architectures are directed by the coordination of CO_3^{2-} ions and the formation of **1** and **2** is controlled by the availability of CO_3^{2-} ions. In both **1** and **2**, the cluster frameworks are of D_{3h} symmetry and comprise a central planar CO_3^{2-} ion which bridges the faces of three distorted $\{M_4(OR)_4\}$ cubanes (R = CH_3 or H), generating an inner planar M_6 ring. In **1a**, the oxygen vertices of each cubane belong to hydroxy ligands, while in **2a** the cubanes contain only methoxy ligands (Figure 1).

The cubane subunits are linked to one another by bridging coordination of the inner-face metal centers of neighboring cubane units, that is, bridging by the central templating carbonate anion and by two acetate ligands (Figure 1). The coordination spheres of the metal centers at the outer-face vertices of each cubane are completed by a bridging acetate ligand (oriented vertically) and two *trans*-tach ligands binding in the expected bis(axial)–mono(equatorial) conformation through the two *cis* amine N positions. The uncoordinated *trans*-amine groups are protonated and thus unavailable for metal complexation but available for hydrogen bonding, effectively rendering the sterically demanding tach unit a terminating group. The geometry of the {Ni$_{12}$} and {Co$_{12}$} clusters is nearly identical, the cubanes of **2a** are very slightly compressed compared to those in **1a**, which leads to a greater separation of the cubanes because the geometry of the central carbonate anion remains constant.

Despite the isostructural nature of the cluster core frameworks, the crystal packing of **1** and **2** is significantly different. Hydrogen bonds between the protonated *trans* amine groups and acetate counterions connect neighboring cluster units. In **1**, the hydroxy ligands in the outer-face cubane vertices also form
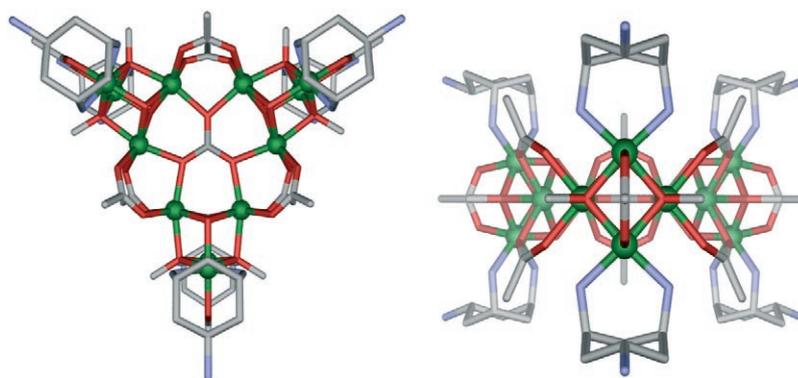
hydrogen bonds with solvent molecules, which is not possible in **2**. This situation leads to a hexagonal crystal system for **1** where the closest *trans*-tach ligands of any three adjacent clusters describe an equilateral triangle while an orthorhombic system is observed for **2** with these *trans*-tach ligands describing isosceles triangles (Figure 2). Therefore the compositional mapping from {Co$_{12}$} to {Ni$_{12}$} structure types can even be monitored crystallographically in the following manner: {Co$_{12}$} to {Co$_8$Ni$_4$}—hexagonal; {Ni$_{12}$} to {Ni$_6$Co$_6$}—orthorhombic.

Low-field magnetic susceptibility data in the range 2–290 K for **2** shows features of both antiferromagnetic and ferromagnetic exchange coupling between the $S = 1$ Ni^{II} centers, resulting in a maximum of χT at 27 K (Figure 3). Preliminary low-temperature high-field magnetization measurements[18] clearly indicate single-ion anisotropy (zero-field splitting, ZFS) contributions owing to spin-orbit coupling and slight ligand-field distortion of the nickel(II) ions, which affects their $^3A_2$ ground states. We were able to reproduce the temperature dependence of the magnetic susceptibility of **2** within an isotropic Heisenberg model that, based on the D_{3h}
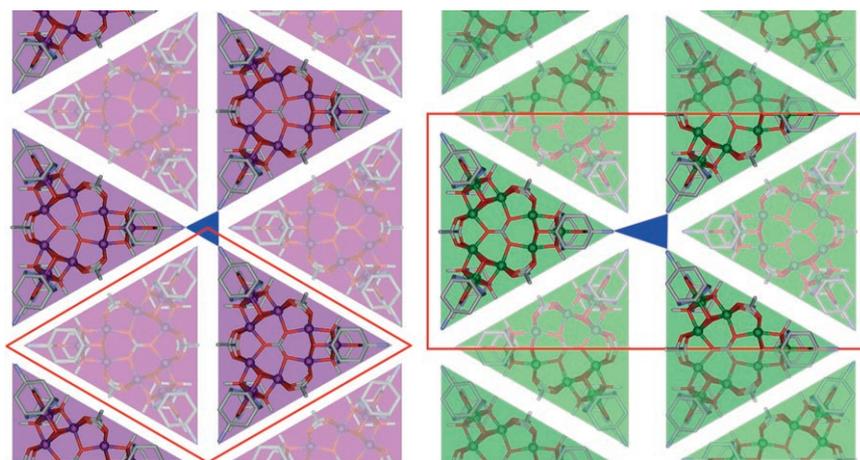
Figure 2. Comparison of the packing of {M$_{12}$} clusters in **1** (left, hexagonal system) and **2** (right, orthorhombic system) within the crystallographic *ab* plane. Red lines show the unit-cell boundaries and blue triangles are used to highlight the geometrical relationship enforced by hydrogen bonding between adjacent clusters. Colors are as in Figure 1.
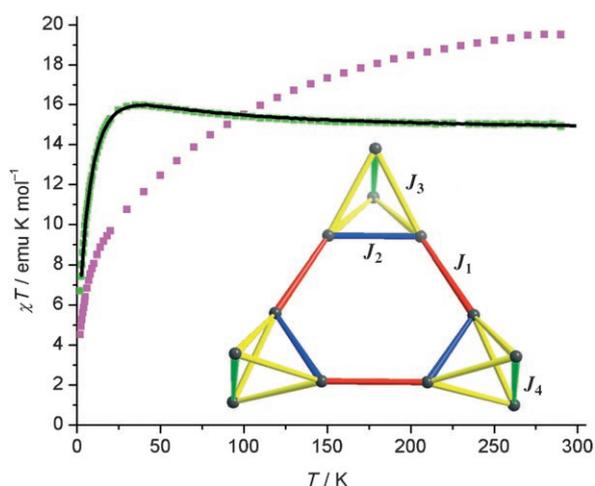
Figure 3. Temperature dependence of χT for **1** (purple squares) and **2** (green squares) at 0.1 T with the best fit to a Heisenberg model for **2** (black line). Inset: Assignment of the exchange parameters J_{1-4} to the M_{12} spin array: J_1 red, J_2 blue, J_3 yellow, J_4 green, see text for details.

symmetry of **2a**, adopts four coupling constants (see inset Figure 3): J_1 (red), between adjacent Ni positions of neighboring Ni_4O_4 cubanes (inter-cubane, mediated by the carbonate and two acetate bridges); J_2 (blue), between the two inner-face Ni positions (two oxo and one carbonato bridges); J_3 (yellow), between inner-face and outer-face Ni positions (one oxo and one methoxy bridge per Ni–Ni contact); J_4 (green), between the two outer-face Ni centers (two methoxy and one acetate bridge). Owing to the complexity of this system with a Hilbert space dimension of 3^{12}, quantum Monte Carlo simulations[19] were performed to scan the parameter space J_{1-4} and g, and the best fit resulted for antiferromagnetic inter-cubane interaction ($J_1/k_B = -17.5$ K) and ferromagnetic intra-cubane interaction with strong variations of the individual exchange strengths, reflecting ferro/antiferromagnetic competition between the involved exchange pathways ($J_2/k_B = 9.5$ K, $J_3/k_B = 1.9$ K, $J_4/k_B = 22.0$ K). The (isotropic) g factor was determined as 2.21, which is a typical value for a Ni^{II} center in a near-octahedral ligand field. Whereas the corresponding χT versus T graph for the $s = 3/2$ Co^{II} derivative **1** does not exhibit a maximum and continually decreases towards lower temperatures (Figure 3), we suspect that the intramolecular coupling is very similar to that established for **2** but is masked by dominating single-ion anisotropy ZFS contributions typical for high-spin $S = 3/2$ Co^{II} in distorted octahedral ligand fields (owing to the splitting of the orbitally degenerate $^4T_1$ ground state into Kramers doublets). A comprehensive model description of **1** will also need to account for the various local ZFS effects by anisotropic exchange in a full spin Hamiltonian. Interestingly, nona-nuclear systems of the type $[M_9(OH)_3(H_2O)_6(HPO_4)_2\text{-}(B\text{-}PW_9O_{34})_3]^{16-}$ (M = Ni^{II}, Co^{II}) comprising similar structural elements—a central C_3-symmetric fragment of three corner-sharing M_3O_9 trimer clusters templated by two central HPO_4^{2-} anions—also feature similar ferromagnetic intra-trimer and antiferromagnetic inter-trimer exchange.[20] Fur-

ther experiments reflecting the local spin distribution of {Ni/Co$_{12}$} intermediates such as high-resolution ESR and MAS-^{1}H NMR spectroscopy are planned.

The pH difference of 2.0 that is necessary for optimal formation and isolation of the pure {Co$_{12}$} and {Ni$_{12}$} cluster species becomes a critical reaction control parameter in the generation of mixed {Ni$_{12-n}$Co$_n$} clusters with a discrete value of n. In the absence of such a differentiating factor the similarity between Co^{II} and Ni^{II} would cause the formation and cocrystallization of a certain range of compositions (i.e. a range of values for n) for a specified stoichiometric Ni:Co ratio. Using this relation, it is indeed possible to isolate all intermediates ($n = 1–11$) as pure compounds, two of which are reported herein: {Ni$_{11}$Co$_1$} (**3**) and {Ni$_6$Co$_6$} (**4**). Since classical analytical methods only can determine the bulk compositions of such compounds and single-crystal X-ray diffraction cannot unambiguously distinguish between single Ni and Co sites, probing the purity of **3** and **4**, that is, the degree of compositional deviations from the stoichiometric Ni:Co average, had to rely primarily on physical-property arguments, differences in the crystal packing, and yield distributions. Based on the susceptibility data for **3** {Ni$_{11}$Co$_1$} we observe a preferred occupation of the metal positions of the outer-face vertices by the single Co^{II} center: If in a first approximation the intramolecular exchange parameters for **2** are employed (i.e. Ni–Ni exchange is equated with Ni–Co exchange) and Co^{II} is approximated as a spin-only $S = 3/2$ center, the two resulting possible population scenarios (the Co center occupies one of the six outer sites (*A*) or one of the six inner sites (*B*)) result in a different temperature dependence of the susceptibility (Figure 4), whereby the experimental curve for **3**, with a clear maximum in χT, is closer to scenario *A*. Likewise, if compound **4** {Co$_6$Ni$_6$} were to actually consist of a 1:1 mixture of {Ni$_{12}$} and {Co$_{12}$} clusters the resulting magnetic susceptibility data would equate to the average of the corresponding individual values for {Ni$_{12}$} and {Co$_{12}$}. However, the susceptibility curve for **4** differs from this average curve, supporting the mass spectrometry data (below) that no such mixture is present (Figure 4, inset).

Further insight is provided, supporting the formation of discrete mixed species, by close examination of the electrospray mass spectrometry data. The spectra for **1** and **2** clearly show envelopes corresponding to the {Ni$_{12}$} and {Co$_{12}$} intact cluster species which can each be assigned as $[Ni_{12}(CH_3O)_{12}\text{-}(CH_3CO_2)_9(CO_3)(tach)_6]^+$ and $[Co_{12}(OH)_{12}(CH_3CO_2)_{10}\text{-}(CO_3)(H_2O)_6(tach)_6(H)]^+$ (Figure 5). Furthermore, the {Co$_6$Ni$_6$} species **4** gives a cryospray (CS) MS envelope which matches that expected for a discrete mixed species (containing $(OH)_6$ and $(CH_3O)_6$ groups), rather than the supposition of many possible outcomes (see Supporting Information). To our knowledge, this is the first time electrospray and cryospray mass spectrometry have been successfully utilized to examine such high-nuclearity, highly labile, first-row transition-metal clusters.

In conclusion, the assembly of large isostructural {Co$_{12}$} and {Ni$_{12}$} clusters is achieved by the use of a selected set of ligands: bridging carboxylate and hydroxy/methoxy ligands as well as templating carbonate ligands, in conjunction with bulky, terminating *trans*-tach groups. In the presented struc-
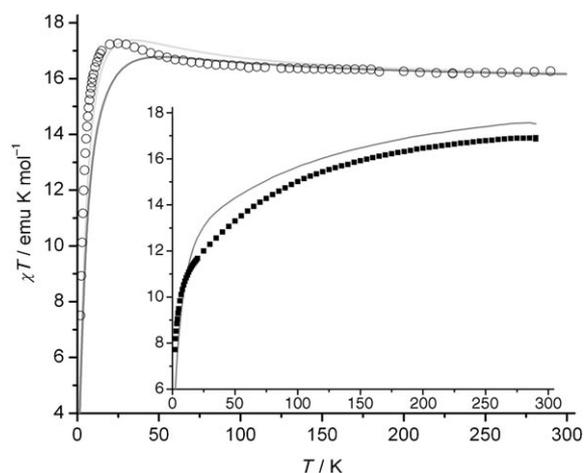
Figure 4. Main plot: Comparison of the experimental χT values of the $\{Ni_{11}Co_1\}$ compound **3** (circles, 1.0 T) with the two possible site-population scenarios, calculated for an approximated spin-only Heisenberg model; *A* (light gray graph; the single Co center occupies one of the six outer metal positions) and *B* (dark gray graph; the Co center occupies one of the six inner metal positions) see text for details. Inset: Comparison indicating qualitative differences between the average χT values of a 1:1 mixture of **1** and **2** (gray graph) with the experimental values of the $\{Ni_6Co_6\}$ compound **4** (squares, 0.1 T).
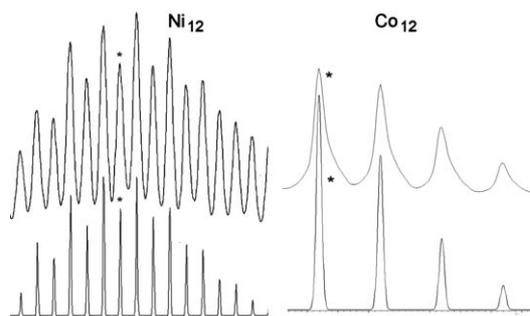
Figure 5. Cryospray mass spectrum for the $\{M_{12}\}$ clusters at $-40°C$. Experimental (top) and simulated data (below). Right: $[Co_{12}(OH)_{12}\text{-}(CH_3CO_2)_{10}(CO_3)(H_2O)_6(tach)_6(H)_1]^+$; * = 2445. Left: $[Ni_{12}(CH_3O)_{12}\text{-}(CH_3CO_2)_9(CO_3)(tach)_6]^+$; * = 2442 (simulated and experimental within 1 Dalton).

tures, *trans*-tach ligands decorate the outer parts of the cubane fragments through bis-chelation through the *cis* amino-groups while the protonated *trans*-amino groups act as hydrogen-bond donors in a supramolecular hydrogen-bonded array in the crystalline state. The similarity in size and coordination character between Ni^{II} and Co^{II} makes the $\{M_{12}\}$ framework suitable for the construction of a series of isostructural mixed Ni–Co clusters, two examples of which were presented. As the reaction parameter space for such mixed-metal coordination clusters is not confined to just the stoichiometric Ni:Co ratio, but involves the acidity of the solution (thereby controlling the OH/OMe ratio), isolation of very pure mixed-metal species is possible.[16] This very narrow distribution curve has been conclusively confirmed by the absence of significant amounts of $\{Ni_xCo_y\}$ cluster cations that deviate from the targeted $\{Ni_6Co_6\}$ composition in electro-

spray mass spectra, and also correlates with the derived magnetism results.

Experimental Section

Synthesis (for full details see the Supporting Information). General remarks, all manipulations involving Co^{II} were performed under nitrogen. **1**: Dilute perchloric acid (13% in water) was used to acidify a solution of *trans*-tach (0.050 g, 0.388 mmol) in methanol (5 mL) to pH 8.5. Addition of Co(OAc)$_2$·4H$_2$O (0.096 g, 0.388 mmol) and sodium carbonate (0.003 g, 0.032 mmol) to this solution gave a dark purple solution which was stirred and then filtered. Hexagonal, red crystals of **1** were obtained in a yield of 11.0% (25 mg, 0.0073 mmol) by diffusion of diethyl ether. Data for **1**:FT-IR (KBr) $\tilde{v}=3420$–3000(s), 2088(m), 1558(s), 1408(s), 1264(w), 1159(w), 1020(m), 932(w), 790(w), 667(m) cm^{-1}; UV/Vis (MeOH, 293 K): 530 nm ($\varepsilon = 640$ mol^{-1}dm^{3}cm^{-1}); elemental analysis calcd (%) for C$_{67}$H$_{183}$Co$_{12}$Cl$_7$N$_{18}$O$_{73}$: C 23.92, H 5.48, N 7.38; found: C 24.60, H 5.00, N 7.40.

2: Addition of Ni(OAc)$_2$·4H$_2$O (0.095 g, 0.388 mmol) and sodium carbonate (0.003 g, 0.032 mmol) to a solution of *trans*-tach (0.050 g, 0.388 mmol) in methanol (5 mL) gave a light green solution of pH 10.5 which was stirred for 1 h and then filtered. Diethyl ether diffusion gave green crystals of **2** in a yield of 14.0% (29 mg, 0.0088 mmol). Data for **2**: FT-IR (KBr) $\tilde{v}=3316$(s), 2175(w), 1560(s), 1164(w), 1048(m), 918(m), 670(m) cm^{-1}; UV/Vis (MeOH, 293 K): 386 nm ($\varepsilon = 211$ mol^{-1} dm^{3}cm^{-1}), 656 nm (119 mol^{-1}dm^{3}cm^{-1}); elemental analysis calcd (%) for C$_{81}$H$_{192}$Ni$_{12}$N$_{18}$O$_{53}$ (-10 MeOH on drying): C 32.75, H 6.52, N 8.49; found: C 32.10, H 7.00, N 9.00.

3: Dilute acetic acid (11% in water) was used to acidify a solution of *trans*-tach (0.050 g, 0.388 mmol) in methanol (5 mL) to pH 10.1. Addition of Ni(OAc)$_2$·4H$_2$O (0.087 g, 0.356 mmol), Co(OAc)$_2$·4H$_2$O (0.008 g, 0.032 mmol) and sodium carbonate (0.003 g, 0.032 mmol) resulted in a light blue-green solution which was stirred for 1 h then filtered. Diethyl ether diffusion gave blue-green diffraction-quality crystals of **3** in a yield of 12.7% (23 mg, 0.0082 mmol). Data for **3**: FT-IR (KBr) $\tilde{v}=3446.2$(vs), 2945.5(m), 2360.4(s), 2340.2(s), 1652.7(s), 1558.2(s), 1418.4(m), 1049.1(m), 668.2(m) cm^{-1}; UV/Vis (MeOH, 293 K): 377 nm ($\varepsilon = 190$ mol^{-1}dm^{3}cm^{-1}), 658 nm ($\varepsilon = 30$ mol^{-1}dm^{3}cm^{-1}); elemental analysis calcd (%) for C$_{81}$H$_{228}$Ni$_{11}$Co$_1$N$_{18}$O$_{71}$: C 29.5, H 6.97, N 7.65; found: C 29.3, H 6.17, N 7.02; FAAS ppm Co 0.22, Ni 1.87, ratio Co:Ni = 1.26:10.74.

4: Dilute acetic acid (11% in water) was used to acidify a solution of *trans*-tach (0.050 g, 0.388 mmol) in methanol (5 mL) to pH 9.3. Addition of Ni(OAc)$_2$·4H$_2$O (0.047 g, 0.194 mmol), Co(OAc)$_2$·4H$_2$O (0.048 g, 0.194 mmol) and sodium carbonate (0.003 g, 0.032 mmol) resulted in a pink solution was stirred for 1 h then filtered. Diethyl ether diffusion gave light red crystals of **4** in a yield of 11.6% (21 mg, 0.0075 mmol). Data for **4**: FT-IR (KBr) $\tilde{v}=3434.6$(vs), 2926.5(m), 1615.1(s), 1568.8(s), 1404.9(s), 1340.3(m), 1163.8(m), 1022.1(m), 920.9(m), 661.5(m) cm^{-1}; UV/Vis (MeOH, 293 K): 540 nm ($\varepsilon = 172$ mol^{-1}dm^{3}cm^{-1}); elemental analysis calcd (%) for C$_{75}$H$_{210}$Co$_6$N$_{18}$Ni$_6$O$_{68}$: C 32.75, H 6.52, N 8.49; found: C 32.10, H 7.00, N 9.00; FAAS ppm Co 0.89, Ni 0.91, ratio Co:Ni = 1.00:1.02.

[1] R. H. Holm, P. Kennepohl, E. I. Solomon, *Chem. Rev.* **1996**, *96*, 2239.

[2] M. Yoshizawa, M. Tamura, M. Fujita, *Science* **2006**, *312*, 251.

Communications

[3] a) M. N. Leuenberger, D. Loss, *Nature* **2001**, *410*, 789; b) F. Troiani, A. Ghirri, M. Affronte, S. Carretta, P. Santini, G. Amoretti, S. Piligkos, G. A. Timco, R. E. P. Winpenny, *Phys. Rev. Lett.* **2005**, *94*, 207208.

[4] a) R. W. Saalfrank, A. Scheurer, I. Bernt, F. W. Heinemann, A. V. Postnikov, V. Schünemann, A. X. Trautwein, M. S. Alam, H. Rupp, P. Müller, *Dalton Trans.* **2006**, 2865; b) J. Schnack, *Lect. Notes Phys.* **2004**, *645*, 155.

[5] R. W. Saalfrank, I. Bernt, M. M. Chowdhry, F. Hampel, G. B. M. Vaughan, *Chem. Eur. J.* **2001**, *7*, 2765.

[6] M. Murugesu, R. Clérac, W. Wernsdorfer, C. E. Anson, A. K. Powell, *Angew. Chem.* **2005**, *117*, 6836; *Angew. Chem. Int. Ed.* **2005**, *44*, 6678.

[7] S. Polarz, A. V. Orlov, M. W. E. van den Berg, M. Driess, *Angew. Chem.* **2005**, *117*, 8104; *Angew. Chem. Int. Ed.* **2005**, *44*, 7892.

[8] See: a) H. Miyasaka, K. Nakata, L. Lecren, C. Coulon, Y. Nakazawa, T. Fujisaki, K.-i. Sugiura, M. Yamashita, R. Clérac, *J. Am. Chem. Soc.* **2006**, *128*, 3770; b) G. Aromi, A. S. Batsanov, P. Christian, M. Helliwell, A. Parkin, S. Parsons, A. A. Smith, G. A. Timco, R. E. P. Winpenny, *Chem. Eur. J.* **2003**, *9*, 5142;

[9] P.-G. Lassahn, V. Lozan, G. A. Timco, P. Christian, C. Janiak, R. E. P. Winpenny, *J. Catal.* **2004**, *222*, 260.

[10] G. Aromi, A. S. Batsanov, P. Christian, M. Helliwell, A. Parkin, S. Parsons, A. A. Smith, G. A. Timco, R. E. P. Winpenny, *Chem. Eur. J.* **2003**, *9*, 5142.

[11] M. Murrie, S. J. Teat, H. Stoeckli-Evans, H. U. Güdel, *Angew. Chem.* **2003**, *115*, 4801; *Angew. Chem. Int. Ed.* **2003**, *42*, 4653.

[12] P. Ayyappan, O. R. Evans, W. Lin, *Inorg. Chem.* **2001**, *40*, 4627.

[13] a) A. J. Blake, C. M. Grant, S. Parsons, J. M. Rawson, R. E. P. Winpenny, *J. Chem. Soc. Chem. Commun.* **1994**, 2363; b) E. K. Brechin, O. Cador, A. Caneschi, C. Cadiou, S. G. Harris, S. Parsons, M. Vonci, R. E. P. Winpenny, *Chem. Commun.* **2002**, 1860; c) G. Wu, R. Clérac, W. Wernsdorfer, S. Qiu, C. U. Anson, I. J. Hewitt, A. K. Powell, *Eur. J. Inorg. Chem.* **2006**, 1927.

[14] X-ray structure analysis and crystallographic data for **1**: $P6_3/mmc$, $a = 21.3178(5)$, $c = 23.3757(6)$ Å, $V = 9199.8(4)$ Å^3, $Z = 2$, $R1 = 0.087$, $wR2 = 0.278$ (all data). **2**: $Cmcm$, $a = 19.8251(7)$, $b = 38.3999(13)$, $c = 23.6258(7)$ Å, $V = 17985.9(10)$ Å^3, $Z = 4$, $R1 = 0.073$, $wR2 = 0.232$ (all data). CCDC-620127 and CCDC-620128 contain the supplementary crystallographic data for this paper. These data can be obtained free of charge from The Cambridge Crystallographic Data Centre via www.ccdc.cam.ac.uk/data_request/cif.

[15] E. Coronado, M. Feliz, A. Forment-Aliaga, C. J. Gómez-García, R. Llusar, F. M. Romero, *Inorg. Chem.* **2001**, *40*, 6084.

[16] This is also confirmed by the generation of a yield map, plotted as function of the Co:Ni ratio against pH (8.5–10.5). Preliminary data demonstrate that only the maximum yield is generated for a given {Co$_x$Ni$_y$} at the precise pH value and {Co$_x$Ni$_y$} ratio.

[17] G. Seeber, D. L. Long, B. M. Kariuki, L. Cronin, *Dalton Trans.* **2003**, 4498; G. Seeber, P. Kögerler, B. M. Kariuki, L. Cronin, *Chem. Commun.* **2004**, 1580.

[18] Preliminary low-temperature (0.4 K) measurements for both compounds **1** and **2** of the magnetization as a function of a (pulsed) magnetic field reveal strong anisotropy that effectively erodes expected spin-level crossings caused by the parabolic form of the lowest multiplet states in the magnetic excitation spectrum; H. Nojiri, unpublished results.

[19] a) O. Syljuasen, A. Sandvik, *Phys. Rev. E* **2002**, *66*, 046701; b) L. Engelhardt, M. Luban, *Phys. Rev. B* **2006**, *73*, 054430.

[20] J. M. Clemente-Juan, E. Coronado, *Coord. Chem. Rev.* **1999**, *193–195*, 361.